Surface Studies of Polyethers with Well-Defined Segmental Length

Chi-Ming Chan*, Lin Li*, Kai-Mo Ng*, Jianxiong Li* and Lu-Tao Weng**
Department of Chemical Engineering*
Advanced Engineering Materials Facility*
Materials Characterization & Preparation Facility**
Hong Kong University of Science and Technology
Clear Water Bay, Kowloon, Hong Kong
P.R. of China

SUMMARY: Two series of polyethers were synthesized by the polymerization of 1, n-dibromoalkane (n = 4, 6, 8, 10, 12, 14 and 18) with bisphenol-A (BA) and 4, 4'-(hexafluoroisopropylidene) diphenol-A. The length of the flexible aliphatic segment changes from 4 Å to 21 Å (corresponding to 4 to 18 CH_2 groups). X-ray photoelectron spectroscopy (XPS), time-of-flight secondary ion mass spectrometry (ToF-SIMS) and atomic force microscopy (AFM) were used to characterize the surfaces of the polyethers. The influence of the length of the flexible aliphatic segments on the surface composition of the BA and 6FBA polyethers was investigated. The intensity ratios of the characteristic SIMS peaks of the flexible segments to those of the rigid segments were related to the length of the flexible segments and the XPS results confirmed that the SIMS intensity ratios can be used to determine the surface compositions. AFM was utilized to investigate the crystallization process of the BA polymer with n = 8. The appearance of nuclei, the generation of primary lamellae and the formation of spherulites were observed dynamically. Nuclei appeared first as 10 nm dots, some disappeared and a few could grow into lamellae. The lamellae that developed from the nuclei bred more lamellae, which in turn induced secondary nucleation and branching of lamellae and finally led to a spherical appearance.

Introduction

The surface segregation in polymers is governed by several factors. The thermodynamic driving force for minimizing the total free energy of the system results in preferential surface segregation of the lower surface energy constituent of the polymer. However, a number of other factors, such as the relative length of the blocks, their sequence length distribution and the concentration of the constituents may also play an important role in the surface composition of copolymers.[1-5] In one of our recent works, the effects of the sequence distribution of poly(acrylonitrile-butadiene) rubbers (NBRs), determined by ^{13}C-NMR, on the surface chemical composition, determined by XPS and dynamic contact angle (DCA) measurements, were studied.[5] The results of XPS and ^{13}C-NMR analyses suggest that surface segregation of the lower surface energy segment (BD) of the NBR copolymers occurs only when the BD segment length is at least equal to the length of the BBB segment and the BBB intensity is above a certain value.

 CCC 1022-1360/00/$ 17.50+.50/0

It has been shown that the secondary ion fragments emitted from a polymer surface are related to the surface molecular structure.[6,7] In particular, ToF-SIMS can provide structural information both in the positive and negative spectra. In order to investigate the effects of the sequence length on the surface composition of a polymer two series of polyethers with a well-defined segment length were prepared, the relationship between the structure of the secondary ion fragments and the surface chemical structure was studied.

Recently, AFM has been applied to study the morphology and kinetic phenomena of polymers.[8,9] In this work, the crystallization process of a semicrystalline polyether with a glass transition temperature near room temperature was studied.

Experiment

The synthesis is described as in Scheme 1:[10]

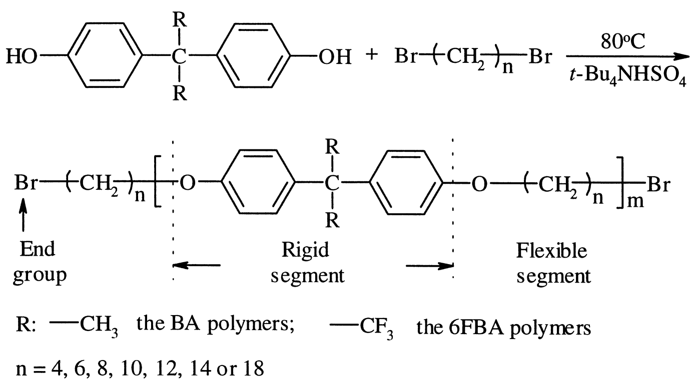

Scheme 1: The preparation of the BA and 6FBA polyethers.

Thin films of the BA and 6FBA polymers were prepared by solution spin casting on silicon wafers. The solvents used for the BA and 6FBA polymers were chloroform and tetrahydrofuran, respectively.

XPS spectra were recorded on a PHI 5600 multi-technique system equipped with an Al monochromatic X-ray source. A pass energy of 58.7 eV was used. The spectra were obtained at a take-off angle of 45°. The ToF-SIMS experiments were performed on a Physical Electronics PHI 7200 ToF-SIMS spectrometer. AFM phase images were obtained using a DI NanoScope III MultiMode™ AFM at room temperature. Si tips with a resonance frequency of ~300kHz were used and the scan rate was 0.8 Hz sec^{-1}.

Results and Discussion

The influence of segmental length on the surface chemical composition

The atomic ratio of F-to-O is plotted as a function of the number of the CH_2 groups, n, as shown in Fig. 1[11]. This ratio is a constant, implying that there is no contamination on the surface of the 6FBA polymers. The concentration of the end groups, Br, is too low to be determined accurately in the BA and 6FBA polymers.

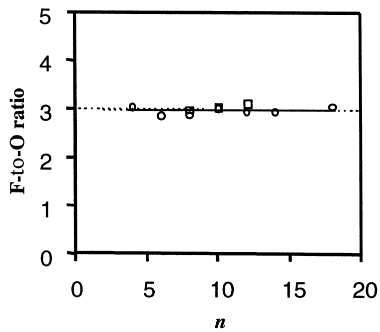

Fig. 1: The F-to-O atomic ratio *vs.* n of the 6FBA polymers

The number of the CH_2 groups, n_s, determined by the C-to-O atomic ratios of the BA and 6FBA polymers, as a function of n, is shown in Fig. 2. The value of n_s of the 6FBA polymers exhibits a linear relationship with the value of n for n = 4 to 18. However, for the BA polymers n_s determined by XPS is much larger than n when $n > 14$. This suggests that the flexible segments segregate onto the surface of the BA polymers when the length of the flexible segment is long enough ($n > 14$, segment length ~17Å). Repeated measurements yielded similar results. A comparison of the XPS results between the BA and 6FBA polymers indicates that the effects of the flexible segment length on the surface composition are different even for the sequential polymers with a very similar structure. The difference in the surface free energy between the rigid and flexible segments is the driving force for the segregation of the low surface component to the surface. Because the BA and 6FBA polymers have a different side group (CH_3 and CF_3), the surface energy difference between the rigid and flexible segments is not identical for these two polymers. The length of the flexible segment plays an important role in determining the surface composition of the polyethers. In the BA polymers, the flexible segment obviously has a lower surface energy than the

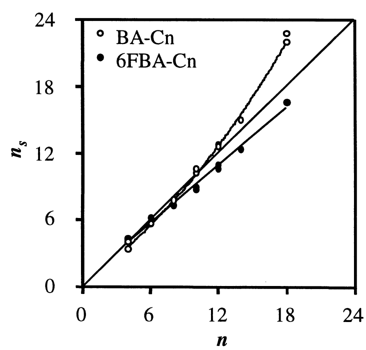

Fig. 2: n_s determined by XPS *vs.* n of the BA and 6FBA polymers

rigid segment. When the length of the flexible segment increases, the mobility of the segment also increases. As a result, surface excess of the flexible segments occurs. But for the 6FBA polymers, the surface energy difference between the rigid and flexible segments may not be significant. Therefore, no significant surface excess of the flexible segments is observed even at n =18.

The influence of the segmental length on the SIMS intensities

The influence of the flexible segment length on the normalized intensity, I_i^N, of the positive aliphatic hydrocarbon ions and the aromatic ions was investigated. The normalized intensity of the characteristic fragments of the flexible aliphatic segments and rigid segments is defined by the following equation:

$$I_i^N = \frac{I_i / I_t}{I_i / I_t(n=4)} \tag{1}$$

where I_t is the total ion intensity, $I_i / I_t(n=4)$ is chosen as the reference and all normalized peak intensities of 6FBA polymers, $(I_i / I_t(n=4)) = 1$. For example, I_i^N of the 6FBA polymers *vs.* n is plotted in Fig. 3. A series of positive aliphatic ion fragments, such as $C_4H_2^+$, $C_4H_3^+$, $C_4H_4^+$, $C_4H_5^+$, $C_4H_6^+$, $C_4H_7^+$, $C_4H_8^+$ and $C_4H_9^+$, at m/z = 50, 51, 52, 53, 54, 55, 56, and 57 were used and the variation of I_i^N can be seen in Fig. 3a.

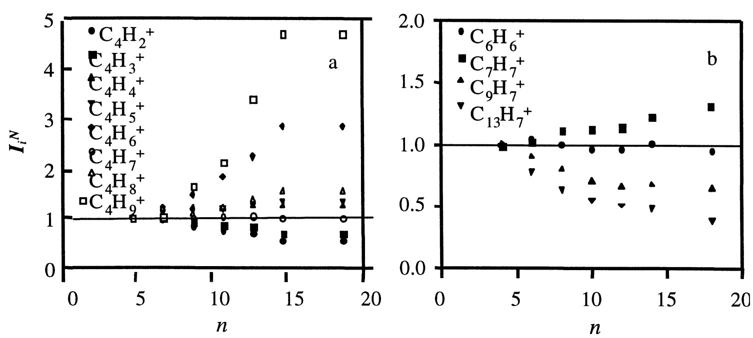

Fig. 3: The influence of the flexible segment length on the intensity of the characteristic positive hydrocarbon ions *vs.* n of the 6FBA polymers. (a) aliphatic secondary ions and (b) aromatic secondary ions.

When the flexible segment length increases, the intensity of the highly unsaturated aliphatic ion fragments, such as $C_4H_2^+$ and $C_4H_3^+$ at m/z = 50 and 51 decreases. However, the intensity of the saturated aliphatic ion, $C_4H_9^+$, at m/z = 57 increases as the flexible segment length increases. This can be explained by the structure of the 6FBA polymers, as shown in Scheme 1. The highly unsaturated aliphatic ions are mainly emitted from the rigid segment and their intensity decreases as the number of the CH_2 group increases. The other unsaturated ions, such as $C_4H_4^+$, $C_5H_5^+$, $C_4H_6^{+,}$ C_4H_7+ and $C_4H_8^+$, are emitted from both the rigid and flexible segments.

The variation of I_i^N of the aromatic ion fragments of the 6FBA polymers, such as $C_6H_5^+$, $C_7H_7^+$, $C_9H_7^+$ and $C_{13}H_9^+$ at m/z = 77, 91, 115 and 165, is shown in Figure 3b. The aromatic ions such as $C_6H_5^+$ and $C_7H_7^+$ can also be emitted from the aliphatic flexible segments. Therefore, they cannot be used as the characteristic positive ions of the rigid segments. However, the larger aromatic fragments, such as $C_9H_7^+$ and $C_{13}H_9^+$, are mainly emitted from the rigid segments; therefore, it is possible to use the intensity of these ions to determine the surface composition of the 6FBA polymers.

In order to simplify the analysis of the ToF-SIMS results, the characteristic ion fragments of the BA and 6FBA polymers are summarized in three series. (1) Flexible fragments, F_i, are mainly emitted from the flexible segment, such as CH_2^-, $C_2H_5^+$, $C_3H_7^+$, and $C_4H_9^+$, at m/z = 14, 29, 43, and 57, respectively. (2) Rigid fragments, R_j, are mainly emitted from the rigid segment, such as $C_7H_{11}O^+$ and $C_{14}H_{13}O_2^+$ at m/z = 135, and 213, respectively, for the BA polymers and $C_9F_6H_5O^+$, $C_{14}F_3H_{10}O_2^+$, $C_9F_5H_4O^-$ and $C_{14}F_3H_8O_2^-$ at m/z=243, 267, 223 and 265, respectively, for the 6FBA polymers. The chemical structures of these ion fragments were reported previously[10]. (3) Molecular fragments, AB_n, are directly related to the structure of the repeat units of the BA and 6FBA polymers, such as $[M\text{-}H]^-$ at m/z = 281, 309, 337, ... with n = 4, 6, 8, ... of the BA polymers. If the bulk effects can be neglected, the ratios of the absolute intensities, $I(F_i)/I(R_j)$, of the flexible fragments to the rigid fragments are related to the number of the CH_2 groups at the surface, n_s, as shown in Eq. 2:

$$\frac{I(F_i)}{I(R_j)} = \frac{S_i \cdot C(F)}{S_j \cdot C(R)} \propto K(ij) \cdot n_s \tag{2}$$

where $I(F_i)$ and $I(R_j)$ are the absolute intensities of the flexible and rigid segments, respectively. S_i and S_j are related to the sensitive factors of the ion fragments i and j, respectively. $C(R)$ and $C(F)$ are the molar concentrations of the flexible and rigid segments, respectively. K_{ij} is a parameter related to the yield of fragments i and j.

To verify Eq. 2, the SIMS results of the BA and 6FBA polymers were analyzed. The intensities of the positive saturated aliphatic ions, such as $C_2H_5^+$, $C_3H_7^+$ and $C_4H_9^+$ at m/z = 29, 43, and 57, $I(F_{29}), I(F_{43}),$ and $I(F_{57})$, were used for the flexible segments of the polymers. For the rigid segments of the BA polymers, the intensities of the characteristic positive ions of the BA polymers $C_9H_{11}O^+$ and $C_{14}H_{13}O^+$ at m/z =135 and 213, $I(R_{135})$ and $I(R_{213})$, were adopted, while for the 6FBA polymers the intensities of the characteristic positive ions of the 6FBA polymers $C_9F_6H_5O^+$ and $C_{14}F_3H_{10}O_2^+$ at m/z =243 and 267, $I(R_{243})$ and $I(R_{267})$, were adopted. As an example, the intensity ratios of the ions for the BA polymers, $I(F_{57})/I(R_{135})$ ($C_4H_9^+/C_9H_{11}O^+$) and $I(F_{57})/I(R_{213})$ ($C_4H_9^+/C_{14}H_{13}O_2^+$), are plotted *vs.* n , as shown in Fig. 4. The intensity ratios, $I(F_{57})/I(R_{135})$ and $I(F_{57})/I(R_{213})$, increase monotonically with n, as shown in Fig. 4a. It is obvious that the ratios do not increase linearly with n. However, the intensity ratios, $I(F_{57})/I(R_{135})$ and $I(F_{57})/I(R_{213})$, increase fairly linearly with n_s as shown in Fig. 4b. The intensity ratios of 6FBA polymers, $I(F_{57})/I(R_{243})$ ($C_4H_9^+/C_9F_6H_5O^+$), and $I(F_{57})/I(R_{267})$ ($C_4H_9^+/C_{14}F_3H_{10}O_2^+$), increase linearly with n. The other intensity ratios,

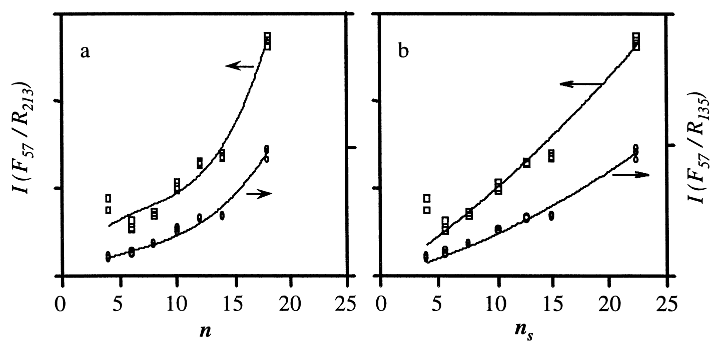

Fig. 4: Intensity ratios of positive ions $I(F_{57})/I(R_{135})$ and $I(F_{57})/I(R_{213})$ for the BA polymers as function of (a) n and (b) n_s.

$I(F_{29})/I(R_j)$ and $I(F_{43})/I(R_j)$, show similar results. These results further reflect the fact that the ratios of the ionic intensities are directly related to the surface concentration of the flexible segments and can be used for quantitative analyzing the surface compositions of these polymers.

Nuclei formation and spherulite growth

AFM was utilized to study the crystallization process and the organization of the spherulite of the BA polymer with n=8.[12] This polymer is attractive for AFM analyses because its glass transition temperature is close to room temperature and its crystallization rate at room temperature allows imaging of the crystallization process with an AFM without a hot stage. The glass transition temperature, melting point, and number–average molecular weight of this polymer were measured to be 6.9°C, 83.5°C, and 5.7×10^3 g/mole respectively. A thin film about 300 nm was prepared by spin casting the polymer solution

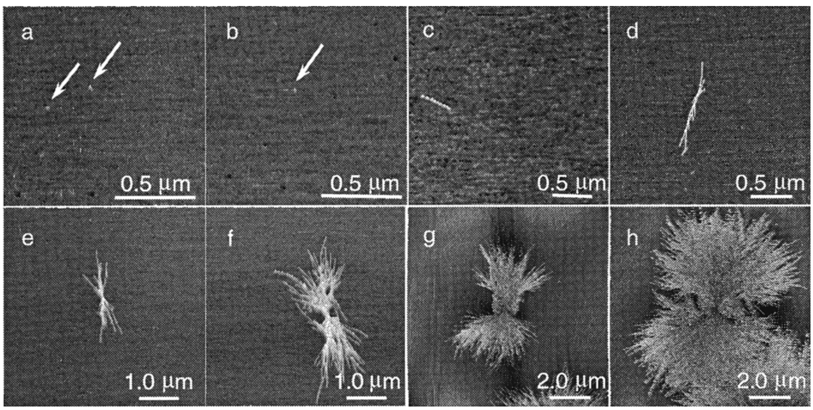

Fig. 5: The formation of a primary nucleus, lamellae and a spherulite

on a silicon wafer and the crystallization process was observed directly under tapping-mode AFM phase imaging, as shown in Fig. 5. Embryos of the lamellae, as fine dots, with a dimension smaller than 10 nm, appeared and disappeared on the surface of the amorphous polymer film during scanning (Figs. 5a and 5b). Figure 5a shows the presence of two embryos. In Fig. 5b, which was obtained approximately 8.7 minutes after the image shown in Fig. 4a, one of the embryos disappeared. We believe that this is the first experimental evidence in a polymer to show that, as predicted by thermodynamics, embryos smaller than a critical dimension are unstable and may not ultimately grow. The initial nucleating lamella grows along the length of the lamella at both ends (Fig. 5c). During the growth stage, it breeds more lamellae (Fig. 5d). When their lengths are longer than 0.5 to 1.0 µm, the lamellae begin to form branches (Fig. 5e) and some lamellae splay apart from each other (Fig. 5f). As a result of continual splaying and branching of the lamellae, the initial lamellae gradually develop into a lamella sheaf and a spherulite skeleton (Figs. 5g, h). We believe that all lamellae except for those in the "eye" of the spherulites are viewed edge-on because the "width" of the lamellae, as viewed in this direction, is approximately 10 nm and this dimension is likely to be the thickness of the lamellae.

It has been suggested that a polymer spherulite develops from a single lamella through unidirectional growth and continuous branching and splaying apart [9, 13)]. Our examination on the development of a lamella embryo into a mature spherulite provides direct evidence to support this view. Furthermore, our experiments revealed that the periphery of the developing spherulites is not as smooth as that observed under optical microscopy. The growth front of the spherulites looks like a hedgehog, as shown in Fig. 5h.

Conclusion

The XPS results indicate that for the low energy segments to segregate on the surface of the polyethers, the segmental length of the low surface energy component has to be above a certain value. The SIMS intensity ratios of the ions from the flexible segments and the rigid segments are related to the surface concentration of the flexible segments as determined by XPS. These findings demonstrate that SIMS data can be used for quantitative analyses of polymer surface. The AFM results provide the direct experimental evidence to show that the embryos of crystalline nuclei are unstable when their dimensions are smaller than a critical value and not all the embryos can ultimately develop into lamellae.

References

1. M. J. Hearn, B. D. Ratner and D. Briggs, *Macromolecules,* **21**, 2950 (1988)
2. M. J. Hearn, D. Briggs, S. C. Yoon, B. D. Ratner, *Surf. Interface Anal.,* **10**, 384 (1987)
3. P. L. Kulmer, H. L. Matteson and Jr., J. A. Gardella, *Langmuir*, **7**, 2479 (1991)
4. X. Chen, Jr., J. A. Gardella, T. Ho and K. J. Wynne, *Macromolecules,* **28**, 1635 (1995)
5. L. Li, C. M Chan and L. T. Weng, *Macromolecules,* **30**, 3698 (1997)

6. D. Briggs, in *Surface Analysis of Polymers by XPS and Static SIMS,* Cambridge University Press, 1998; L. Li, C. M Chan and L. T. Weng, *Macromolecules,* **30**, 3698 (1997)
7. C. M. Chan, in *Polymer Surface Modification and Characterization,* Hanser, New York, 1994
8. R. Pearce and G. J. Vancso, *Polymer*, **39**, 1237 (1998)
9. D. A. Ivanov and A. M. Jonas, *Macromolecules*, **31**, 4546 (1998)
10. L. Li, C. M. Chan, K. M. Ng and L. T. Weng, *Macromolecules* (submitted).
11. L. Li, C. M. Chan, S. Liu, L. An, K. M. Ng, L. T. Weng and K. C. Ho, *Macromolecules* (submitted)
12. L. Li, C. M. Chan, J. X. Li, K. M. Ng, K. L. Yeung and L. T. Weng, *Macromolecules* **32,** 8240 (1999)
13. R. H. Olley and D. C. Bassett, *Polymer* **30**, 399 (1989)